COBEM 2023 27TH INTERNATIONAL CONGRESS OF MECHANICAL ENGINEERING

ABCM Brazilian Society of Mechanical Sciences and Engineering
27th ABCM International Congress of Mechanical Engineering
December 04-08, 2023, Florianópolis-SC, Brazil

COB-2023-2050
EXPERIMENTAL STUDY OF LOST CIRCULATION USING NON-NEWTONIAN FLUIDS IN FRACTURED POROUS MEDIA

Cássio L. Schneider
Felipe B. Pereira
Fernando C. De Lai
Silvio L. M. Junqueira
Universidade Tecnológica Federal do Paraná – UTFPR, Centro de Pesquisas em Reologia e Fluidos Não Newtonianos – CERNN, Curitiba-PR, Brasil, 81280-340.
cassioschneider@alunos.utfpr.edu.br, felper@alunos.utfpr.edu.br, fernandodelai@utfpr.edu.br, silvio@utfpr.edu.br

Alex T. A. Waldmann
André L. Martins
Centro de Pesquisas da PETROBRAS – CENPES, Interação Rocha-Fluido, Rio de Janeiro-RJ, Brasil, 21941-915.
awaldmann@petrobras.com.br, aleibsohn@petrobras.com.br

Abstract. *Research on the flow of non-Newtonian fluids through porous ducts or channels has garnered significant attention due to its wide range of practical applications in engineering, such as the extraction, production, and retrieval of oil and gas reserves. Specifically, during well drilling operations, a drilling fluid with distinct non-Newtonian properties is pumped, interacting with the porous interface of the well-formation system. The presence of fractures or fissures in the porous formation, whether naturally occurring or induced, can result in lost circulation. This condition amplifies fluid loss and poses a threat to the well's integrity. In this study, the flow of non-Newtonian fluids through a partially porous and fractured channel, aiming to understand and characterize the phenomenon of lost circulation. The tests presented were performed in an experimental set-up, comprising a rectangular test section, representing a well-formation set with a transverse fracture, instrumented with pressure, flow rate and temperature gauges to monitor flow. Non-Newtonian fluids were formulated by mixing water with three different concentrations of Carbopol,10, 15 and 20%, resulting in solutions with different apparent viscosities. The fluid flow curves were fitted according to the Herschel-Bulkley model. Porous substrates with 10 and 20 pores per inch represented the surrounding rock formation. The results show that all parameters can change the pressure settings during the lost circulation, exerting a direct influence on the differential pressure generated between the vertical channel and the fracture.*

Keywords: *lost circulation, experimental set-up, fractured channel, porous media, non-Newtonian fluids*

1. INTRODUCTION

In oil reservoirs, oil and natural gas are originally produced by generating rocks and later migrate, mainly through capillary effects and buoyancy forces, to reservoir rocks that are rocks with void inside (porous). The constituents extraction from the reservoir rocks encompasses different processes, among which it stands out the drilling (Gray and Darley, 1980).

The drilling is performed by the rotational movement of a drill that compresses and grinds the rock, generating a lot of gravels. The outcoming cuttings are removed continuously due to the drilling fluids which is injected into the drill column and returns to the surface through the annulus region between the substrate walls and the drilling column (Azar and Samuel, 2007).

In addition to removing cuttings, the drilling fluid must perform a number of other functions, such as keeping the cuttings in suspension, stabilizing the well walls by controlling the pressure of the rock formation, cool and lubricate the drill string assembly and transmit hydraulic power to the drill bit. To perform all necessary functions, the viscosity of the drilling fluids varies with the shear rate and for this reason they are classified as non-Newtonian (Bourgoyne Jr et al., 1991).

The drilling may damage the wall and the rock formation that surrounds it. Such damage, that appears in the form of cracks and fractures, is due to the high-pressure gradients associated to the process, which facilitates the fluid invasion towards the formation as the porous substrate gets fractured. Therefore, a phenomenon rather undesirable for the oil industry, so called lost circulation, takes place. The lost circulation is defined as the drilling fluid that flows towards the rock formation through the pores or cracks in the well-formation set, which is aggravated since a preferential flow is verified if the formation is fractured (Cook et al., 2012; Ezeakacha et al., 2018).

The objective of this work is to investigate experimentally the fluid loss process in a partially porous and fractured channel, using non-Newtonian fluids, in order to analyze the influence of flow and working fluid parameters on the differential pressure generated along the fracture. Results show the influence of variations of the fluid apparent viscosity and porous substrate over the lost circulation process. For that, parameters such as the circuit flow rate, the channel gradient pressure, the differential pressure at the fracture and the fluid temperature are monitored.

2. PROBLEM FORMULATION

Operations in the oil and gas industry have a high complexity of parameters commonly associated to geometry and operating conditions. In order to make the analysis possible some assumptions must to be done.

The problem geometry encompasses the well-formation set, as can be seen in Figure 1(a), in which the well is considered vertical with a discrete fracture (discontinuity) in a horizontal plane. Therefore, the well crosses the fracture plane perpendicularly.

As the main objective of this study is to investigate the fluid loss in the well annulus region, the flow inside the drilling string is disregarded. Thus, the region of interest comprises the annular region and the fractured formation, where the drilling fluid flows upwardly interacting with the porous formation and the fracture.

The Figure 1(b) shows the simplifications considered and the dashed line delimits the region of interest for the present study. The channel width, h_{CH} [m], represents the dimension of the well annulus region, the fracture region is represented by a thickness, e_{FR} [mm], and a length h_{FR} [m]. With regards to the vertical channel, the length upstream and downstream the fracture are represented by l_{UP} [m] and l_{DW} [m], respectively.

In this context, the present work investigates the fluid lost circulation by both fracture and rock formation considered porous.

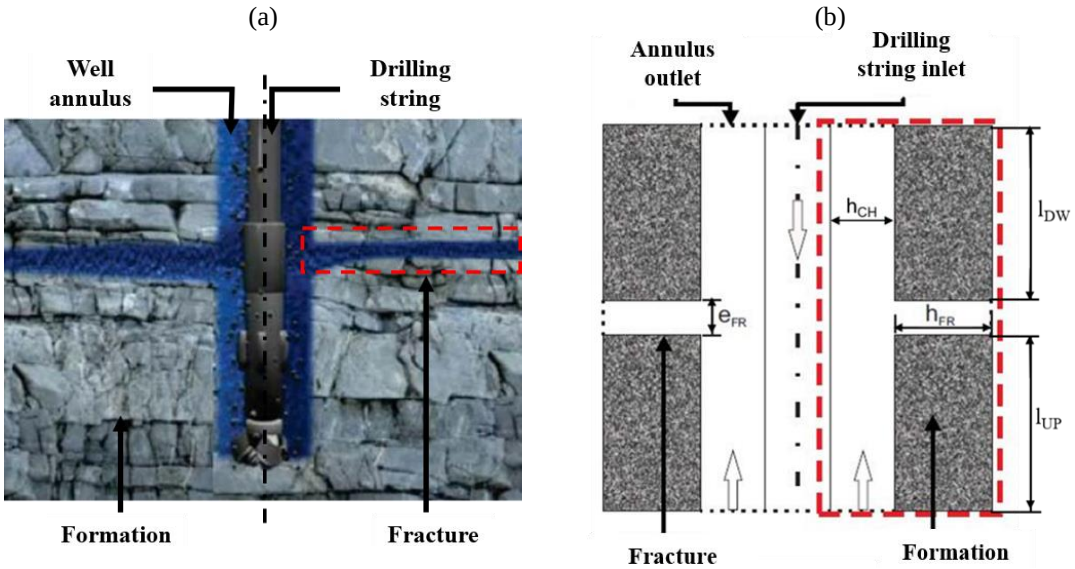

Figure 1. Simplifications: (a) well-fracture set idealization and (b) region of interest.

3. EXPERIMENTAL PROCEDURE

The tests were performed in an experimental set designed and built to characterize the lost circulation phenomenon in a partially porous and fractured channel, in order to analyze the effect of the rock formation during the process, allowing the use of non-Newtonian fluids and the monitoring of variables such as flow, pressure and temperature during the experimental tests.

Figure 2(a) shows the hydraulic circuit diagram and Figure 2(b) shows the key components of the experimental set installed on the Porous Media Lab dependencies (LaMP) at the Research Center for Rheology and Non-Newtonian Fluids (CERNN – UTFPR). The experimental set consists of a tank with mixer (E-1) to homogenize the aqueous solution, in which there is a T type thermocouple to measure the solution temperature during the tests. A screw pump (E-2) provides the flow through the entire circuit. After leaving the pump the solution reaches the test section (E-3). The test section presents two exits, one at the upper nozzle, where the solution passes through a Coriolis type mass flowmeter (I-1) designed to measure the mass flow rate in real time. In the other exit, at the end of the fracture, there is valve with electric actuator (V-2) to control flow rate at the fracture end. The fluid is redirected to the tank via two hoses (T-5 and T-8) which have larger diameters than the outlets, so that the pressures are atmospheric.

The test section, designed to represent the well annulus region, has one of the faces made of acrylic to allow the visualization not only of the flow through the porous media but also along the fracture. The section has a rectangular cross section of 60x16mm and 2m long. In order to measure the local pressure, the section has two relative pressure transducers:

one (I-3) located 0.24m from the channel inlet and the other (I-4) located near the channel outlet (1.78m) above the fracture. Figure 3(a) shows the transducers position and the test section dimensions. The fracture is located 1.27m from the vertical channel inlet to ensure a fully developed flow. The channel width represents the dimension of the annular region, for a well opening with outer and inner diameter, of 8.5 and 5 inches, respectively. Such dimensions are based on a given step of the drilling process, as suggested by Calçada et al., (2015) and Cayeux et al., (2018).

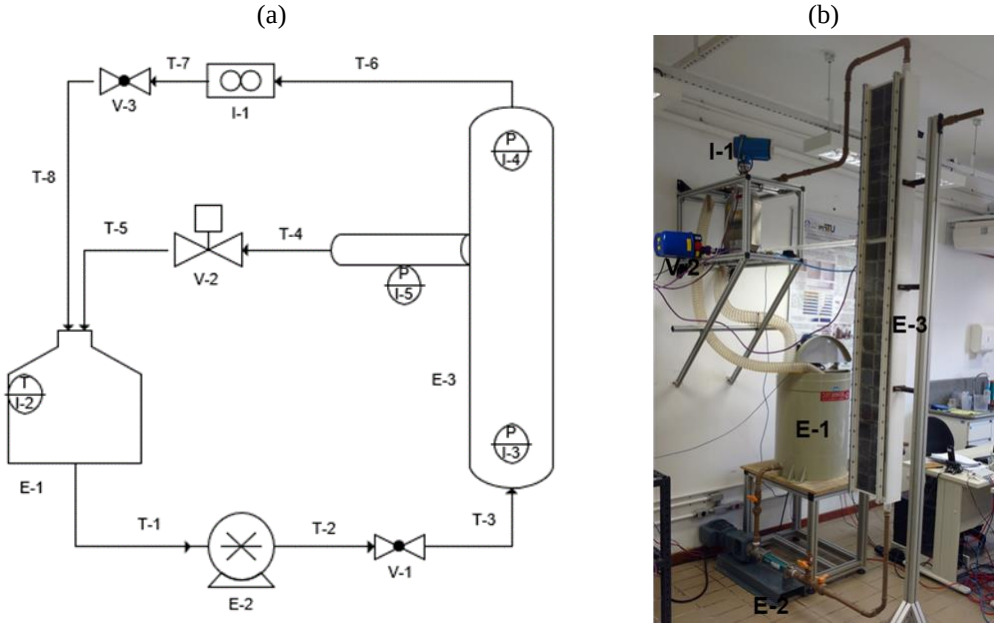

Figure 2. Experimental set: (a) hydraulic circuit diagram and (b) overview of the key components.

The fracture is extended through a rectangular channel 16 x 16 mm and 1 meter long, as can be seen in Figure 3(b). The fracture thickness is based on the fracture measurements found in the drilling process (between 2 and 45 mm), as presented by Almagro et al. (2014), and the length was determined in order to allow the analysis of the differential pressure generated in the fracture with the variation of the evaluated parameters. The differential pressure transducer used has two pressure measurement points, one at the center of the channel and the other at the end of the fracture.

The rock formation is represented by crosslinked foam ceramic filters having linear porous concentration of 10 and 20 porous per inch (PPI). Blocks of 87x87x16 mm are arranged along the entire test section upstream and downstream of the fracture. Porous samples are connected 4 by 4 using silicone, as can be seen in Figure 3(c). The Figure 3(d) shows the test section filled with porous material to represent the rock formation, standing out the region (1) as the free channel for the fluid flow, the region (2) as the rock formation (porous material), and the region (3) as the beginning of the discontinuity in the well formation (fracture).

Three Carbopol aqueous solutions with different concentrations (10, 15 and 20%) used as working fluid provided different apparent viscosity ranges for the same standard shear rate of 1000 s^{-1} (η_{1000}). Fann 35 A viscometer was used to obtain the apparent viscosity from the flow curve. The rheology tests performed on the same day of the lost circulation tests, at an ambient temperature of 20ºC, aimed to reduce temperature variation effects and possible fluid degradation. In Table 1, the nomenclature of the tested fluids indicates the substance added to water (CBP) with the approximated apparent viscosity (η_{1000}) of the working fluid obtained for the standard shear rate and ρ is the fluid's specific mass. The flow curves of non-Newtonian fluids were adjusted according to the Herschel-Bulkley model, Eq.1, as suggested by the literature (Di Giuseppe et al., 2015). Figure 4 shows the flow curves for fluids CBP10, CBP10*, CBP15, CBP20 and CBP20*, as well as the equations obtained by the Herschel-Bulkley adjustment made to the non-Newtonian fluids. The * represents a fluid made at a different time, but with the same polymer concentration. Table 2 summarizes the parameters resulting from the adjustments, where τ_0 is the Herschel-Bulkley fluid's yield limit stress [Pa], k is the consistency index [Pa.s^n] and n represents the power law index.

Table 1. Solutions used during the experimental tests characterized at 20ºC.

Fluid	Concentration [%]	ρ [kg/m^3]	η_{1000} [cP]
CBP05	10	1019.6	4.86
CBP10	15	1020	9.91
CBP10*	15	1020	10.88
CBP20	20	1020.2	20.40
CBP20*	20	1020.2	19.62

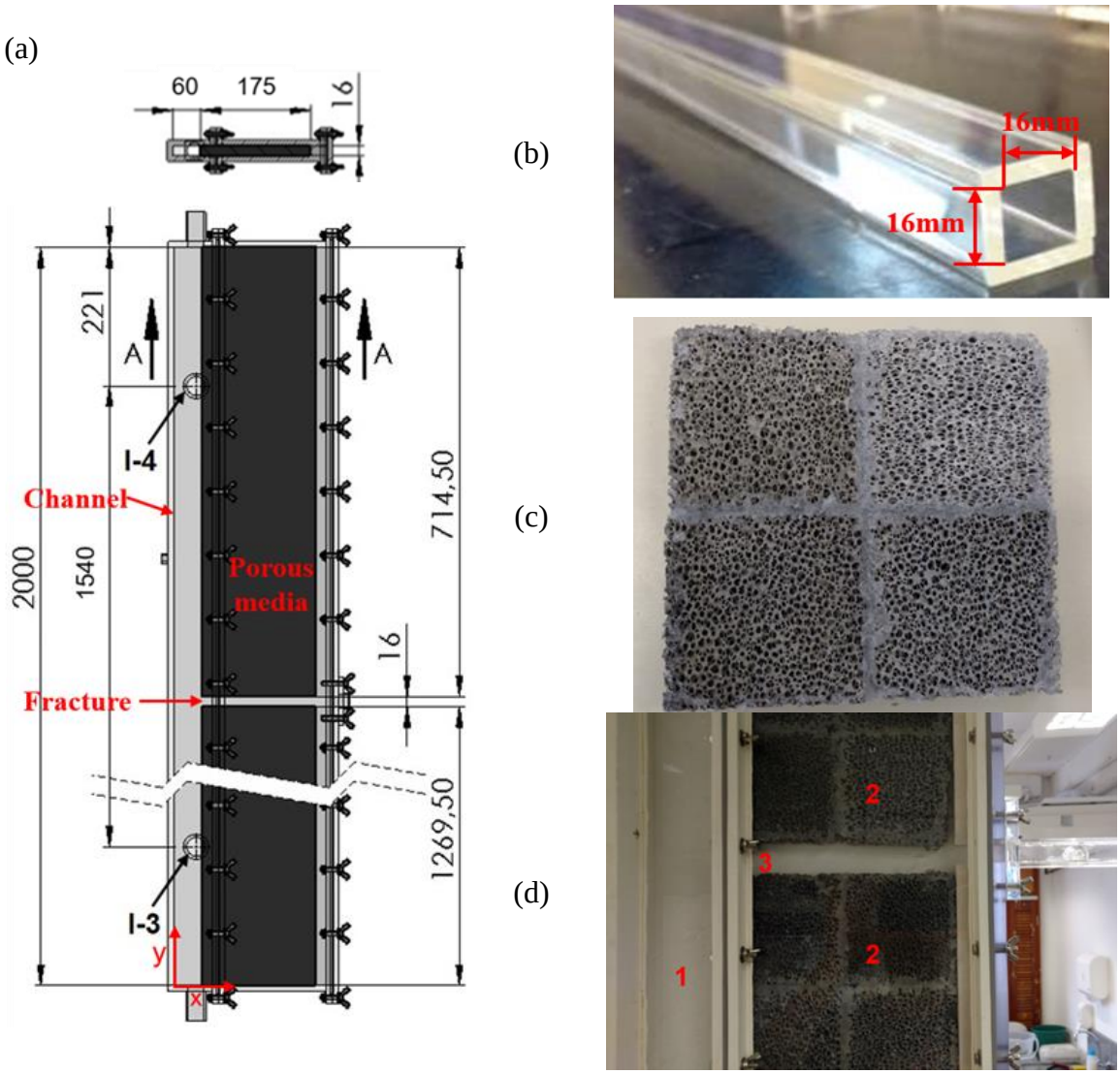

Figure 3. Test section: (a) dimensions in millimeters, (b) fracture extension, (c) porous samples and (d) coupled section.

$$\tau = \tau_0 + k\dot{\gamma}^n \text{ for } |\tau| \geq |\tau_0|$$
$$\dot{\gamma} = 0 \text{ for } |\tau| < |\tau_0| \qquad (1)$$

Before releasing the fluid through the experimental circuit, it is necessary to homogenize the fluid in the tank (E-1) for 1 hour then start the pump to begin the flow throughout the circuit, keeping the control valve at the tip of the fracture closed. The flow rate is adjusted for the desired Reynolds number through real-time monitoring by LabVIEW software. The Reynolds number for the Herschel-Bulkley modeled fluids is given by Eqs. 2 and 3 (Madlener et al., 2009), where u expresses the fluid's average velocity [m/s], Dh is the hydraulic diameter of the vertical channel [m], and m is defined as the local gradient between the ratio of shear stress and strain rate.

The fluid's specific mass and rheological parameters (i.e., the consistency index, the fluid power law index and the yield limit stress) are furnished to LabView to calculate the Reynolds number as a function of the flow velocity in the test section. With the vertical channel flow defined, the monitoring and recording of the measured parameters follow. After 30 seconds, the control valve is activated, allowing the mixture to flow through the fracture at the predetermined flow rate. The measured flow rate at the section exits and the pressure variation along the fracture change and over time, these variables stabilize. From this moment on, as there is no further change in the flow rate and fracture pressure, the measurements cease, ending the test.

$$Re_{HB} = \frac{\rho \bar{u}_{pl}{}^{2-n} D_h{}^n}{\left(\frac{\tau_0}{8}\right)\left(\frac{D_h}{\bar{u}}\right)^n + k\left(\frac{3m+1}{4m}\right)^n 8^{n-1}} \qquad (2)$$

$$m = \left(\frac{nk\left(\frac{8\bar{u}}{D_h}\right)^n}{\tau_0 + k\left(\frac{8\bar{u}}{D_h}\right)^n} \right) \qquad (3)$$

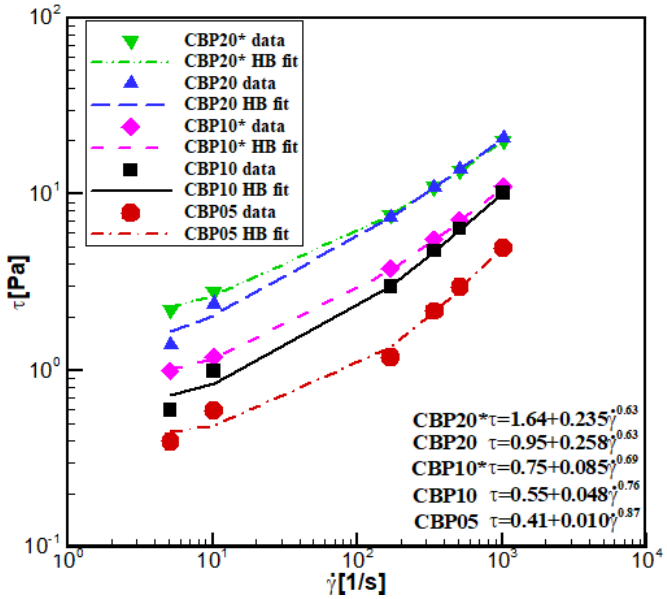

Figure 4. Flow curves and HB adjustments for the working fluids at 20ºC

Table 2. Constants obtained for the HB adjustments made from the experimental data.

Fluid	τ_0 [Pa]	k [Pa.s^n]	n [-]
CBP05	0.41	0.010	0.87
CBP10	0.55	0.048	0.76
CBP10*	0.75	0.085	0.69
CBP20	0.95	0.258	0.63
CBP20*	1.64	0.235	0.63

4. RESULTS AND DISCUSSION

In this section the influence of the flow Reynolds number (Re), fracture outlet flow rate (Q_{FR}), fluid apparent viscosity (η_{1000}) and porous substrate (MP) on the differential pressure generated along the fracture is investigated. Table 3 shows the range of parameters to be varied in the subsequent sections. For the sake of comparison, the highlighted parameters correspond to the base case. The lost circulation tests were conducted with laminar and fully developed flow when the fluid reaches the fracture entrance. The monitoring parameters are the return flow rate (Q), the pressure gradient in the channel ($\Delta p/\Delta x$) and the differential pressure at the fracture (p_{dif}).

Table 3. Range of experimental parameters.

Reynolds number	Re	[-]	100; **200**
Fracture outlet flow rate	Q_{FR}	[%]	5; 10; **30**; 50
Fluid apparent viscosity	η_{1000}	[cP]	5; **10**; 20
Porous substrate	MP	[PPI]	10; **20**

Figure 5(a) shows results in triplicate of the return flow behavior (Q), that is, the channel outlet flow as a function of time, for the standard configuration of Table 3 (MP20 porous substrate, CBP10 fluid, Re = 200 and Q_{FR} = 30%). Note the steep drop-off of Q when the fracture is opened, at t = 30s, which diverts 30% of the initial flow (Q_i) to the fracture ($Q = Q_i - Q_{FR}$). Before and after the fracture opening, the flow rate remains constant and there is practically no difference between the tests, proving the pump's effectiveness in providing constant flow rate. The fracture is closed at t = 150 s, and Q recovers its initial values. Triplicate results of Figure 5(b) display the behavior of the differential pressure (p_{dif}) between the center of the channel and the fracture end over time. Differential pressure increases due to fracture opening but stabilizes after approximately t = 50s. The similar behavior observed in the three tests guarantees the efficacy of the experimental procedure. Therefore, in the following results, an average of the three tests of each configuration is performed.

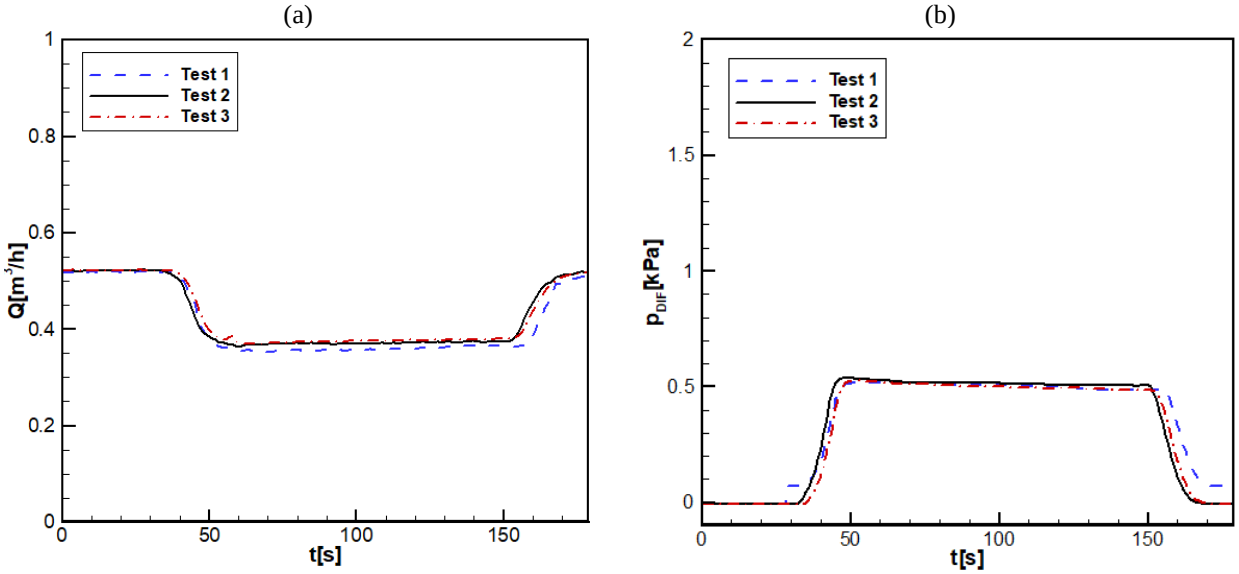

Figure 5. Triplicate of the base test MP20, CBP10, Q_{FR} = 30% and Re = 200: (a) return flow rate; (b) fracture differential pressure.

Still considering the base configuration, Figure 6 shows the pressure gradient between the upstream and downstream of the fracture entrance (Δp/Δx). The low value of fracture output flow (Q_{FR} = 10%) produces a Δp/Δx practically constant throughout the test. However, high values of Q_{FR} (30 and 50%) imply a slight decrease in the pressure gradient. Such a decrease occurs as the pressure drop caused by the horizontal flow in the fracture is smaller than the pressure drop of the vertical flow on the fracture entrance upstream region. The higher the flow rate through the fracture, the vertical channel pressure decreases more markedly at the inlet than at the outlet. The vertical channel pressure gradient behavior is similar regardless of the other parameters variation.

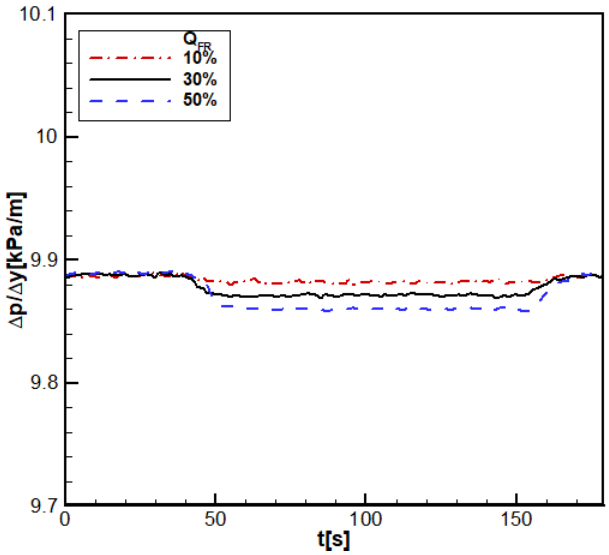

Figure 6. Channel pressure gradient over time for the base test MP20, CBP10 and Re = 200.

4.1 Fluid apparent viscosity influence

To analyze the fluid apparent viscosity effect (η_{1000}), three different concentrations of aqueous Carbopol solutions (CBP) in water were used as working fluid (10, 15 and 20%) using MP20 as porous matrix, Re = 100 and Q_{FR} = 30%. All viscosity values (~ 5, 10 and 20 cP) obtained in the rheological tests considered a shear rate of $1000s^{-1}$ as reference. Considering the inability of the pump to deliver a flow rate high enough to reach Re = 200 with CBP20 fluid, and the high pressures observed in higher viscosity fluids, the number of Re = 100 was used as a limit to preserve the integrity of the test section.

Figure 7(a) displays the time evolution of the return flow rate (Q). The higher the working fluid polymer concentration, the higher the flow rate needed to reach Re = 100. This behavior is because the higher the viscosity, the greater the flow viscous friction effects. Figure 7(b) shows the corresponding time evolution of the differential pressure (p_{dif}) along the

fracture. As expected, the high viscosity and yield stress (τ_0) of the CBP20 fluid (Table 2) imply high pressures, even before fracture flow begins. As the flow in fracture starts, the differential pressures along the fracture increase proportionally to the fluid's viscosity. The higher the polymer concentration, the higher the pressure level reached at the instant the measurements stabilize.

Figure 8 shows the initial ($Q_{AVE,I}$) and final ($Q_{AVE,F}$) average values of the return flow rate and the corresponding initial ($p_{AVE,I}$) and final ($p_{AVE,F}$) fracture differential pressure as a function of the fluid apparent viscosity of the formulated fluids. These values represent the mean of the measurements of ($Q_{AVE,I}$) and ($p_{AVE,I}$) concerning the initial 30s of each test, as well as for the final 30s before the fracture closure ($Q_{AVE,F}$ and $p_{AVE,F}$). The solid and dashed lines represent the initial and the final values, respectively. Results evidence the higher flow rate needed for the CBP20 fluid and the practically linear pressure variation along the fracture with the working fluid polymer concentration.

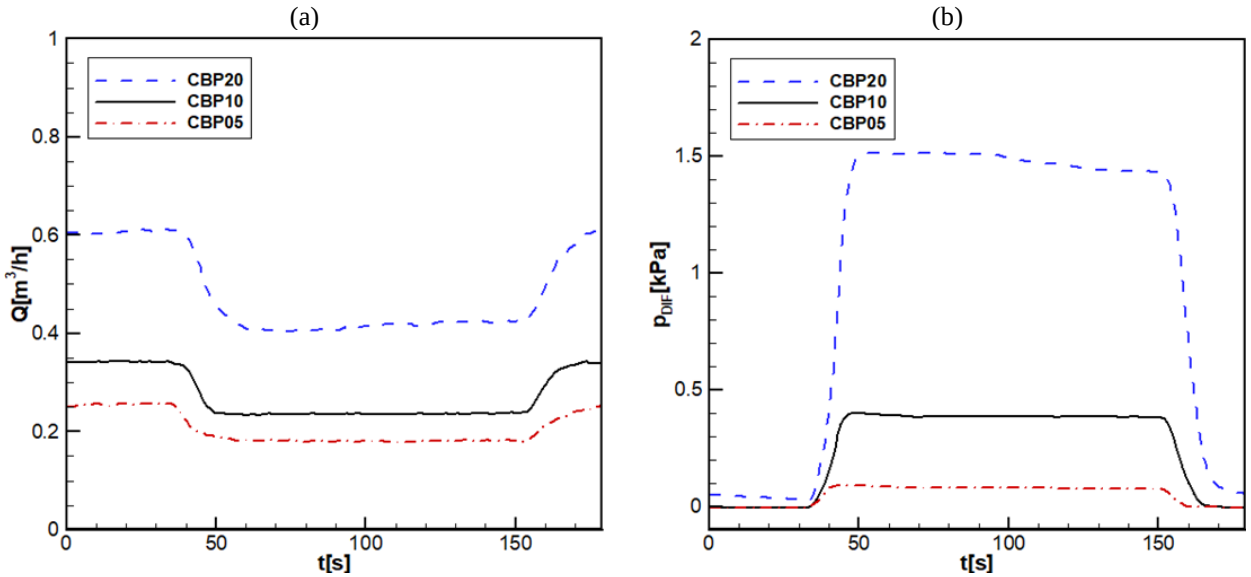

Figure 7. Time evolution of the measured parameters during the tests with different working fluid, MP20, Re = 100 and Q_{FR} = 30%: (a) return flow rate; (b) fracture differential pressure.

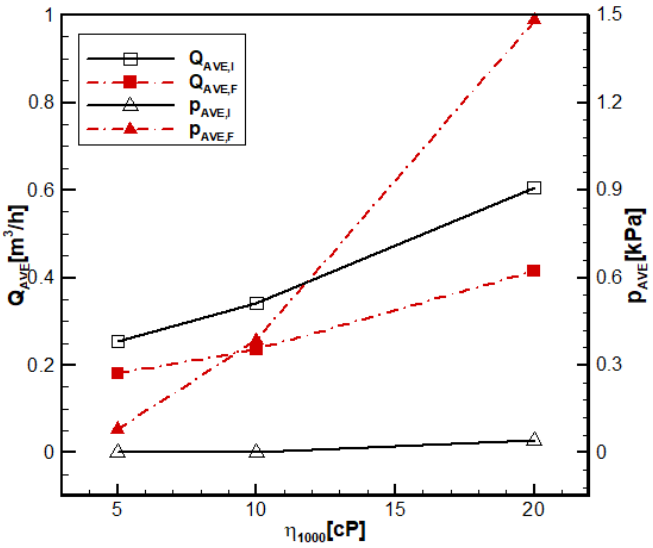

Figure 8. Return flow rate and fracture differential pressure variation as a function of fluid apparent viscosity for MP20, Re = 100 and Q_{FR} = 30%.

4.2 Porous substrate influence

To evaluate the effect of porous substrate, experiments considered two reticulated foam ceramic filters, with linear porous concentration of 10 and 20 pores per inch (PPI), respectively the MP10 and MP20 porous matrices, considering Re = 100 and three values of fracture flow rate Q_{FR} (5, 30 and 50%). Initially, tests were carried out using the CBP20*, the most viscous of the others tested, regardless of the shear rate. Figure 9(a) shows the time evolution for the return flow

rate (Q) and Figure 9(b) the corresponding variation in the differential pressure p_{dif} along the fracture for the same instants. The valve at the fracture end was kept open for 180 seconds.

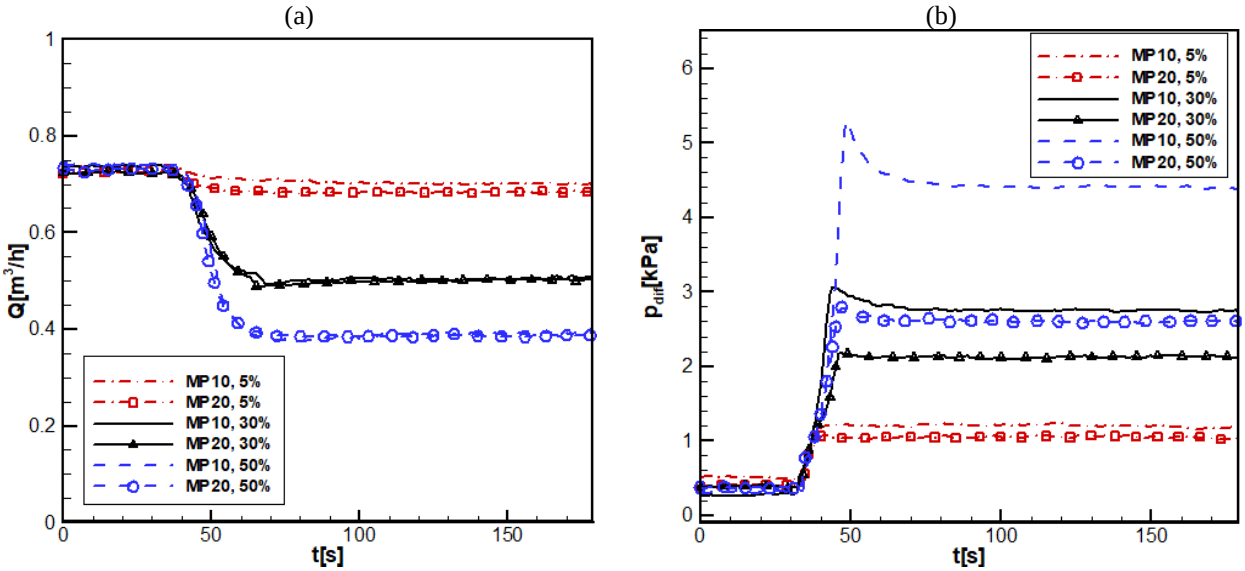

Figure 9. Time evolution of the measured parameters during the tests with different porous substrates, CBP20*, Re = 100 and Q_{FR} = 5, 30% and 50%: (a) return flow rate; (b) fracture differential pressure.

The differential pressure referring to the CBP20* fluid is higher for substrate MP10 than MP20, regardless of the fracture outlet flow rate. Furthermore, the higher the output flow, the more significant the difference between the differential pressure for both porous matrices. A larger pore throat allows a more considerable amount of fluid to percolate through the porous medium, generating a more substantial pressure increase along the fracture. This behavior is even more evident when analyzing the average return flow rate (Q_{AVE}) and the differential pressure (p_{AVE}) as a function of the fracture outlet flow rate (Q_{FR}) for different pore throat values, as shown in Figure 10. The dashed-dotted line, which represents the increase in differential pressure for MP10, grows more intensely than the dashed line, which means the same rise for MP20 substrate.

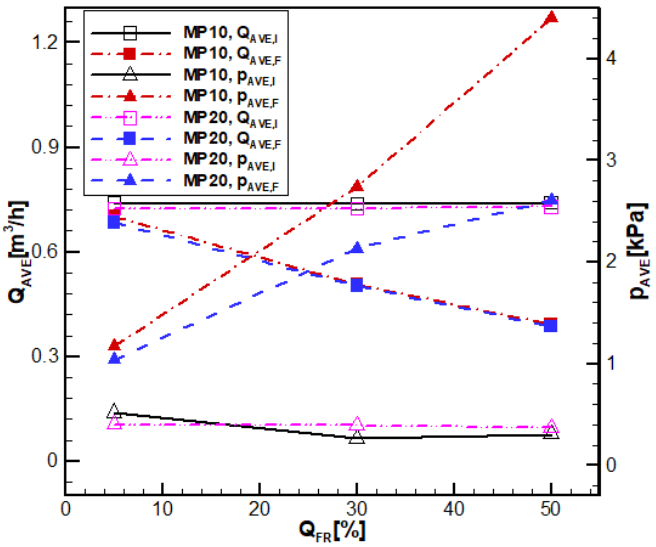

Figure 10. Return flow rate and fracture differential pressure variation as a function of the fracture outlet flow rate for different porous substrates with CBP20* and Re = 100.

Considering Q_{FR} (5, 30, and 50%), CBP10* fluid, and raising Reynolds number to 200, Figure 11(a) and Figure 11(b) show, respectively, Q and p_{dif} as a function of time. As Re increases, Figure 11(b) shows that the differential pressures in the MP10 and MP20 substrates are similar for fracture outflow rates (Q_{FR}) of 5 and 30%, while for Q_{FR} = 50%, MP20 has a more significant pressure gain. This behavior can be better observed in Figure 12, which compares the average initial and final values of the return flow and the differential pressure. The dashed line (MP20) and the dashed-dotted line (MP10) with filled deltas overlap for the 5% and 30% fracture outlet flow rates. However, for Q_{FR} = 50%, the differential pressure growth using the MP20 substrate is more accentuated. Thus, since the fluid velocity in the channel is higher, the

results show no significant differences in the flow through the porous medium for Q_{FR} = 5 and 30%. Additionally, for a high flow rate (Q_{FR} = 50%), the pressure loss due to the greater restriction of the MP20 substrate in relation to the MP10 is the main factor responsible for the pressure differential along the fracture, considering that a greater amount of fluid is forced to flow through the porous medium.

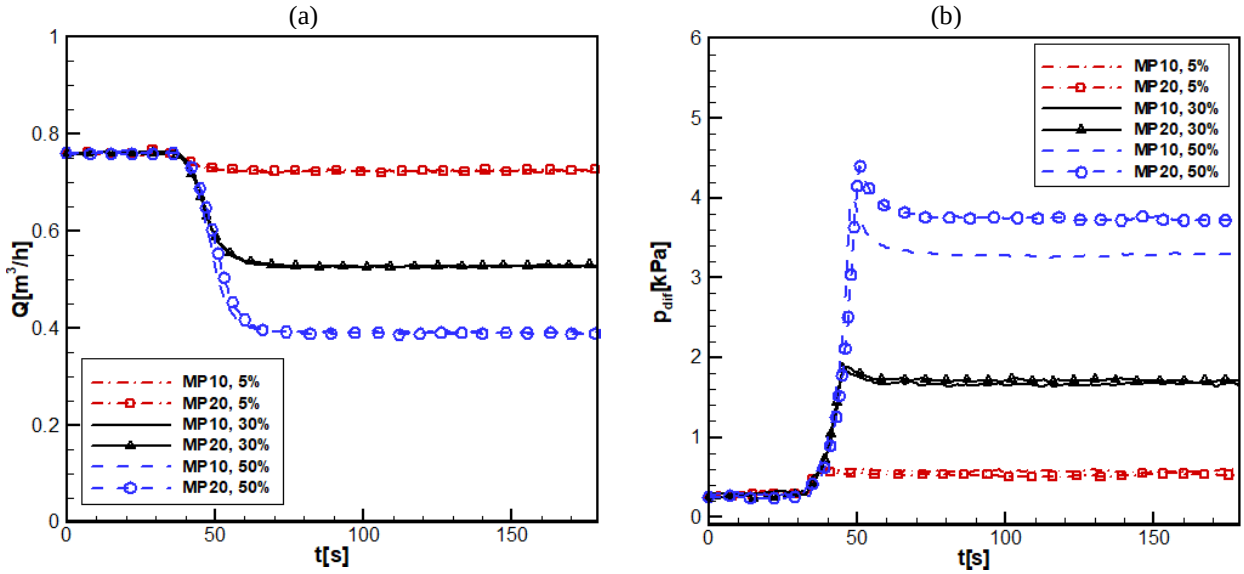

Figure 11. Time evolution of the measured parameters during the tests with different porous substrates, CBP10*, Re = 200 and Q_{FR} = 5, 30% and 50%: (a) return flow rate; (b) fracture differential pressure.

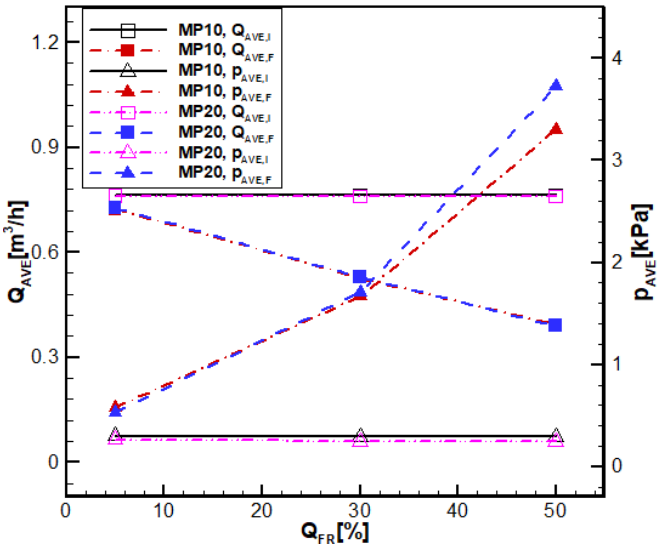

Figure 12. Return flow rate and fracture differential pressure variation as a function of the fracture outlet flow rate for different porous substrates with CBP10* and Re = 200.

Comparing the substrate pore throats results, it is concluded that two factors influence the pressure loss generated as the lost circulation takes place. One refers to the fact that the porous medium with a larger pore throat (MP10) facilitates the flow through the pores. In this way, when the fluid loss through the fracture begins, more fluid flows through the matrix MP10 than the matrix MP20, so the differential pressures are higher. Therefore, the more significant pressure drop generated in the MP10 substrate is evident for higher viscosities, as it allows a greater flow rate in the porous region. Another aspect concerns the case with the highest channel Reynolds number (Re = 200) and, mainly, the highest flow rates through the fracture (Q_{FR} = 50%), where the amount of fluid flowing through the porous medium is similar, regardless of the substrate pore throat. The MP20 matrix results in a greater fluid loss because it restricts the flow more than the MP10 case, when the fluid is forced to flow towards the porous medium. Therefore, the smaller the pore throat, the greater the resulting pressure loss, consequently, the higher the observed differential pressures.

5. CONCLUSIONS

This work investigated experimentally the loss of non-Newtonian fluids due to a transverse fracture in a partially porous vertical channel. The non-Newtonian fluids were formulated by mixing water with three different concentrations of Carbopol, providing different apparent viscosity ranges. Porous substrates with 10 and 20 PPI linear porous concentration played the surrounding formation role. The results considered the effect of vertical channel Reynolds number, fracture outlet flow rate, working fluid apparent viscosity, and porous substrate on return flow rate and the fracture differential pressure.

The increase in the pressure along the fracture is proportional to the increase of the polymer concentration and consequent fluid apparent viscosity enlarge in a practically linear manner, considering the Carbopol concentrations used of 10, 15 and 20%.

The porous medium with a larger pore throat facilitates the flow through the pores, so the differential pressures are higher. However, for the highest channel Reynolds number and, mainly, the highest flow rates through the fracture porous media with smaller pore throat, by restricting more the flow, generate higher pressure loss and consequently higher differential pressures.

6. ACKNOWLEDGEMENTS

The authors are grateful to the Nacional Agency of Petroleum, Natural Gas and Biofuels (ANP), the Human Resources Program for the Petroleum and Gas Sector PRH-ANP (PRH21.1 – UTFPR), the Coordenação de Aperfeiçoamento de Pessoal de Nível Superior – Brasil (CAPES) and CENPES-PETROBRAS for the provided financial support.

7. REFERENCES

Almagro, S. P. B.; Frates, C.; GARAND, J.; MEYER, A. Sealing fractures: Advances in lost circulation control treatments. Oilfield Review Autumn, v. 26, n. 3, p. 4–13, 2014.

Azar, J. J; Samuel, G.R., 2007. “Drilling Engineering,” Tulsa: PennWell Corporation.

Bourgoyne Jr, A. T.; Millheim, K. K.; Chenevert, M. E.; Young JR, F. S., 1991. Appplied Drilling Engineering. 2. ed. Richardson, TX: SPE.

Calçada, L. A.; Duque Neto, O. A.; Magalhães, S. C.; et al. Evaluation of suspension flow and particulate materials for control of fluid losses in drilling operation. Journal of Petroleum Science and Engineering, v. 131, p. 1–10, 2015. Elsevier.

Cayeux, E.; Shor, R.; Aambrus, A.; et al. From shallow horizontal drilling to ERD wells: How scale affects drill ability and the management of drilling incidents. Journal of Petroleum Science and Engineering, v. 160, p. 91–105, 2018. Elsevier B.V.

Cook, J.; Growcock, F.; Guo, G.; Hodder, M.; Van Oort, E., 2012. “Stabilizing the Wellbore to Prevent Lost Circulation,” Oilfield Review, v. 23, n. 4, p. 26–35.

Di Giuseppe, E.; Corbi, F.; Funiciello, F.; et al. Characterization of Carbopol® hydrogel rheology for experimental tectonics and geodynamics. Tectonophysics, v. 642, n. 1, p. 29–45, 2015. Elsevier B.V.

Ezeakacha, C. P.; Salehi, S.; Kiran, R. Lost circulation and filter cake evolution: Impact of dynamic wellbore conditions and wellbore strengthening implications. Journal of Petroleum Science and Engineering, v. 171, n. August, p. 1326–1337, 2018. Elsevier B.V.

Gray, G. R.; Darley, H. C. H., 1980. Composition and Properties of Oil Well Drilling Fluids. 4. ed. Houston, TX: Gulf Publishing Company.

Madlener, K.; Frey, B.; Ciezki, H. K. Generalized Reynolds number for non-Newtonian fluids. Progress in Propulsion Physics, v. 1, p. 237–250, 2009.

8. RESPONSIBILITY NOTICE

The authors are the only responsible for the printed material included in this paper.